G-1-05

Wrangling Spin-Orbit-Torque Voltage-Controlled-Oscillator

Zhifeng Zhu*[§a], Gaurav Gupta*[δa], Hsin Lin[b,c], Gengchiau Liang[a,b]

[a] Department of Electrical and Computer Engineering, National University of Singapore, Singapore-117576
[b] Centre for Advanced 2D Materials and Graphene Research Centre, National University of Singapore, Singapore 117546
[c] Department of Physics, National University of Singapore, Singapore 117542
Tel: (65) 6516 2898, Email: {[§]a0132576@u.nus.edu, [δ]elegg@nus.edu.sg}, *equal contribution

Abstract

We posit a novel principle for designing spin-orbit-torque (SOT) oscillator controlled via voltage input (VCO) which has large output power, ranging from −24 to −38 dBm, wide frequency tunability from 3.4 GHz to 6.2 GHz, and low power consumption (below 1.5 mW). The effect of physical and electronic control parameters on the device operation is also expounded. The proposal provides new insights for taking spintronic oscillator into RF applications.

1. Introduction

VCO generates periodic oscillations whose period can be controlled via voltage input. VCO, as part of phase-locked loop, is the main component of frequency synthesizer used in RF transceiver for frequency modulation and demodulation. Conventional CMOS VCOs, e.g. ring oscillator and LC tank oscillator, have problems of large silicon area, large power dissipation, and small frequency tunability [1]. To overcome these problems, recently spin-torque nano-oscillator (STNO) has been proposed with small area (~ area of magnetic tunnel junction (MTJ)), less power dissipation, as well as large frequency tunability [2]. STNO, however, suffers from low output power (~ −85 dBm i.e. ~18 μV peak voltage) and large phase noise [3]. Therefore, lack of high output power, wide-band spintronics oscillators stands as a critical bottleneck in commercialization of spin-oscillator technology.

To solve this problem, in this work, we propose a scheme of spin-torque based VCO (Fig. 1(a)) with oscillation frequency ranging from 3.4 GHz to 6.2 GHz, which covers the requirements of RF, and with output power ranging from −24 dBm to −38 dBm. In a three-terminal MTJ placed over HM, we work out the criteria which empowers the device with VCO functionality with much larger output power due to near full-swing in FL's magnetization (M_{FL}) compared to standard spin-hall effect (SHE) or STT based STNOs which have limited swing of M_{FL} (theoretical max. 50%).

2. Methodology

Magnetization dynamics in the MTJ has been appraised by integrating Landau-Lifshitz-Gilbert-Slonczewski (LLGS) equation via fourth-order Runge-Kutta method for CoFeB MTJ [4] in macrospin approximation. The multiple-reflection mechanism has been taken into account to obtain the STT efficiency [5]. Furthermore, demagnetization tensor [6] and dipole field coupling tensor [7] are computed via analytical expressions for rectangular magnets. A linear roll-off of TMR to zero with voltage bias of 1 V has been assumed. The output signal amplitude V_{pk} and frequency has been calculated by taking Fast Fourier Transform (FFT) of the output signal V_O, and output power computed as $10+20\log_{10}(|V_{pk}|)$.

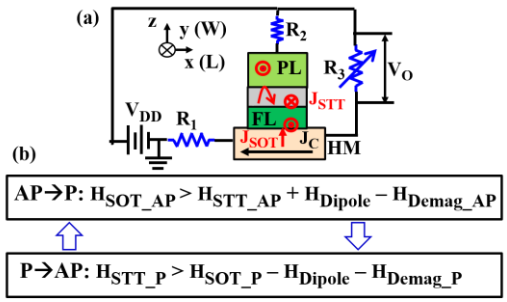

Fig. 1. (a) Device structure for appraising SOT-VCO. Length (L), width (W) and thickness (t) of rectangular magnets of pinned-layer (PL) (free-layer (FL)) are 50, 60 and 4 (3) nm respectively. MTJ parameters [4]: RA=1.5x10^{-12} Ω-m^2, zero-bias TMR=150% and 1 nm thick MgO. Tungsten heavy metal (HM) has {L,W,t} = {55, 66, 4.5} nm. R_3=2.3 KΩ. R_1 and R_2 provide additional controls but shorted (1Ω) in this work. (b) Operation principle illustrating the wrangling among the effective fields of pure-spin current induced SOT (H_{SOT}), spin-polarized current induced STT (H_{STT}), H_{Dipole} (effect of PL field on FL), and H_{Demag} (internal to FL). **This loop-back criteria determines the frequency range of VCO**.

3. Operation Mechanism and Discussion

The magnetization oscillation is guaranteed by the combined effect of shape anisotropy field ($H_{Demag}(\pm\hat{y})$), dipolar field ($H_{Dipole}(+\hat{y})$), and effective field generated by STT ($+\hat{y}$) and SOT ($-\hat{y}$). STT and SOT effects wrangle with each other, and assisted with dipolar field from PL and demagnetization field in FL enable a sustained astable switching of FL, because of which MTJ resistance and current through all nets oscillate, an effect which we read as voltage change across R_3.

Weak shape-anisotropy along y-axis assisted with H_{Dipole} ensures stable antiparallel (AP) state (FL along $+\hat{y}$) when device is switched-off. When turned-on, SOT and H_{Demag} tend to switch FL to $-\hat{y}$, while STT and H_{Dipole} resist such switching. Note that since transfer-torque efficiency (η) in AP state is larger than in P state, hence despite of smaller MTJ current because of AP state (than in P state), STT strongly resists the switching. At large enough V_{DD}, current through HM is large enough to overcome it to switch FL to $-\hat{y}$. Now, as MTJ gets into P state, current through both MTJ and HM increase, but η decrease. Hence, STT alone is insufficeint to switch back FL. STT, H_{Dipole}, and H_{Demag} together tend to drag FL back to $+\hat{y}$, and MTJ into AP state, while SOT opposes this change. In order to satisfy these two conditions (Fig. 1(b)), the resistance, supply voltage, and device dimensions are carefully optimized to enable self-sustained oscillations.

Fig. 2(a) shows the I-V characteristics where the stable

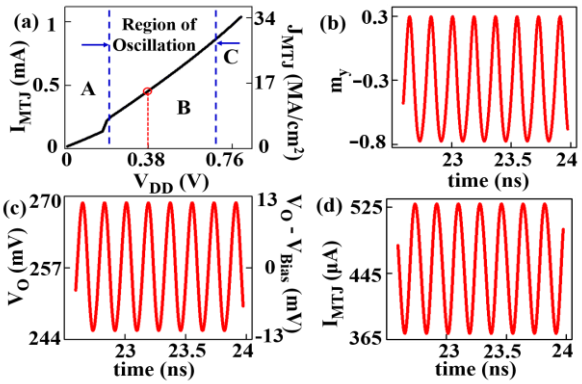

Fig. 2. (a) I-V characteristics of device with MTJ current (I_{MTJ}) on left y-axis and current density (J_{MTJ}) on right. Sustained oscillations for an exemplar case of V_{DD}=0.38 V for FL magnetization unit vector component along y-axis m_y (b), output voltage V_O (left y-axis) (c), output voltage swing without operating bias (right y-axis) (c) and I_{MTJ} (d).

oscillation region is between 0.18 and 0.67 V based on Fig. 1(b). On the other hand, below V_{DD}=0.18 V, the combined field of STT and H_{Demag} is not enough to initiate the switching from $+\hat{y}$ to $-\hat{y}$, and above V_{DD}=0.67 V, the oscillation is not stable and decays to another stable point. Fig. 2(b)-(d) demonstrate the functionality by showing the magnetization, output voltage, and MTJ current oscillation at representative operating voltage V_{DD} of 0.38 V. The observed peak-to-peak value of V_O is 25 mV which is significantly larger than noted for STNO [3].

Fig. 3(a) illustrates the appraisal of the performance metric of the device i.e. frequency tunability, output power (P_O) and power consumption ($P_{Consumed}$) across V_{DD}. Inset of Fig. 3(a) shows the frequency spectrum by taking FFT of 375 cycles of V_O for V_{DD}=0.38V. The fundamental frequency locates at 4.84 GHz and a weak second harmonic at 9.9 GHz, indicating that the output signal is not a pure sinusoid. This can be understood from FL dynamics governed by LLGS equation. V_O and fundamental tone for all V_{DD} in Fig. 3(a) is extracted from respective FFT. Frequency is observed to be in the range from 3.4 GHz to 6.2 GHz. The increase of frequency becomes more gradual at high voltage. Fig. 3(b) shows how the power consumption and output power relate to V_{DD}. The energy efficiency, defined as the ratio of output power (red-triangle) to the consumed power (black-circle), is observed to drop as V_{DD} increases. Note that in the entire range, power consumed is less than 1.5 mW which is much lower than CMOS based VCOs (~10 mW at 3 GHz) [8]. Furthermore, as the area of this VCO is just HM area which is nearly same as MTJ area, this design is expected to have

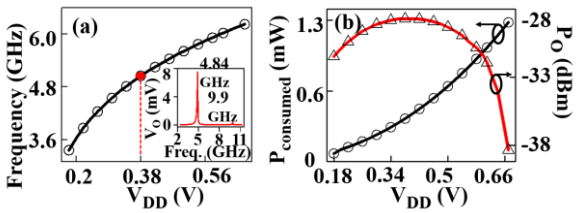

Fig. 3. (a) Oscillation frequency versus V_{DD} with frequency spectrum of V_O at V_{DD} = 0.38V in inset. (b) Power consumption (left y-axis) and Output power across V_{DD}.

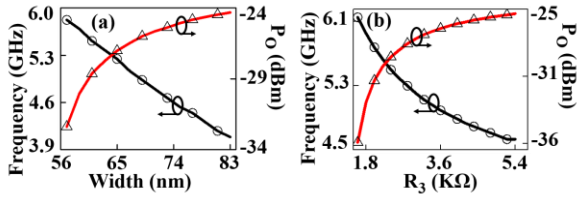

Fig. 4. Oscillation frequency and output power versus MTJ width (a) and resistance R_3 (b).

smaller area than CMOS VCOs designed using multiple transistors, for instance an n-stage ring-oscillator needs at least n PMOS and n+1 NMOS transistors. Therefore, this design can indeed serve as low power VCO while maintaining high performance. Moreover, the output power (Fig. 3(b)), ranging of −28 to −38 dBm, is much higher than STNO (~ −85 dBm) which are currently being researched as replacement for CMOS VCOs because of small MTJ area.

Finally, the effect of MTJ width and resistance R_3 on oscillation frequency and output power are investigated in Fig. 4. The width has been swept from 57 nm to 83 nm, ensuring that easy-axis along y-axis and astable oscillations in device are maintained. The increase in MTJ width reduces the frequency while enhancing the output power as shown in Fig. 4(a). This trend is induced by the change in the demagnetizing field (weakens along y-axis as the magnet becomes more stable along y-axis) and the dipole field (weakens along y-axis) which results in a new balance among the four fields (above two with H_{STT} and H_{SOT}). In Fig. 4(b), R_3 is swept from 1.8 to 5.4 KΩ beyond which there is no stable oscillation. Increasing R_3 reduces both HM and MTJ current thereby weakening both STT and SOT fields, hence reducing (increasing) the oscillator frequency (output power). These results show both MTJ width and R_3 as effective controls for designing and tuning oscillator frequency.

4. Conclusion

A novel scheme of spin-torque VCO has been promulgated in this work, with large operation window (V_{DD} from 0.18 to 0.67 V), and frequency ranging from 3.4 GHz to 6.2 GHz for chosen design parameters. The power consumption (< 1.5 mW) is much lower than CMOS VCOs (~10 mW) at similar frequency (3 GHz). Furthermore, the output power, from −24 to −38 dBm, is much larger than STNOs (−85 dBm). Effect of MTJ width, R_3 and V_{DD} as physical and electronic parameters are studied to provide deeper insights into the device operation. These results should enable the design and applications of energy-efficient, small area and high output power VCOs, especially in RF applications.

Acknowledgments

This work at the National University of Singapore was supported by CRP award no. NRF-CRP12-2013-01.

Reference: [1] L. Dai et al. ISBN: 978-1-4613-5414-7, Springer (2003). [2] S. E. Russek et al., Chap. 38, Functional Nanomaterials, CRC press (2010). [3] H. S. Choi et al., Sci. Rep. 4, 5486 (2014). [4] Y. Nagamine eta l., APL 89 (16), 162507 (2006). [5] W. Zhu et al., SPIN 5 (1), 1550003 (2015). [6] A. Aharoni, JAP 83, 3432 (1998). [7] R. Engel-Herbert, et al. JAP 97, 074504 (2005). [8]. C. Richard, et al. IEEE-TED 1768 (2016).